Structural Engineering and Mechanics, *Vol. 60, No. 1 (2016) 51-69*
DOI: http://dx.doi.org/10.12989/sem.2016.60.1.051

Ductile cracking simulation procedure for welded joints under monotonic tension

Liang-Jiu Jia[1a], Toyoki Ikai[2b], Lan Kang[**3], Hanbin Ge[*2] and Tomoya Kato[2c]

[1]Research Institute of Structural Engineering and Disaster Reduction, College of Civil Engineering, Tongji University, Shanghai, 200092, China
[2]Department of Civil Engineering, Meijo University, 1-501 Shiogamaguchi, Tenpaku-Ku, Nagoya, 468-8502, Japan
[3]School of Civil Engineering and Transportation, South China University of Technology, Guangzhou, 510640, China

(Received January 4, 2016, Revised May 26, 2016, Accepted July 12, 2016)

Abstract. A large number of welded steel moment-resisting framed (SMRF) structures failed due to brittle fracture induced by ductile fracture at beam-to-column connections during 1994 Northridge earthquake and 1995 Kobe (Hyogoken-Nanbu) earthquake. Extensive research efforts have been devoted to clarifying the mechanism of the observed failures and corresponding countermeasures to ensure more ductile design of welded SMRF structures, while limited research on the failure analysis of the ductile cracking was conducted due to lack of computational capacity and proper theoretical models. As the first step to solve this complicated problem, this paper aims to establish a straightforward procedure to simulate ductile cracking of welded joints under monotonic tension. There are two difficulties in achieving the aim of this study, including measurement of true stress-true strain data and ductile fracture parameters of different subzones in a welded joint, such as weld deposit, heat affected zone and the boundary between the two. Butt joints are employed in this study for their simple configuration. Both experimental and numerical studies on two types of butt joints are conducted. The validity of the proposed procedure is proved by comparison between the experimental and numerical results.

Keywords: ductile fracture; true stress-true strain; butt weld; cracking; structural steel

1. Introduction

Welded steel moment-resisting framed (SMRF) structures have been once considered as one of the most effective systems, while confidence in this structural system was shaken by the fact that a great number of the prequalified welded beam-to-column connections failed due to brittle fracture during the 1994 Northridge earthquake (Hajjar *et al*. 1998, Mahin 1998, O'Sullivan *et al*. 1998)

*Corresponding author, Professor, E-mail: gehanbin@meijo-u.ac.jp
**Co-corresponding author, Associate Professor, E-mail: connielan@tom.com
[a]Ph.D., E-mail: lj_jia@tongji.edu.cn
[b]Graduate Student, E-mail: 120437061@ccalumni.meijo-u.ac.jp
[c]Graduate Student, E-mail: tomoyan0514@gmail.com

http://www.techno-press.org/?journal=sem&subpage=8 ISSN: 1225-4568 (Print), 1598-6217 (Online)

and the 1995 Kobe (Hyogoken-Nanbu) earthquake (AIJ 1995, Bruneau *et al*. 1996, Kuwamura Lab 1998, Nakashima *et al*. 1998). However, the failure modes in the two earthquakes are distinguished from each other, where cracks commonly initiated at weld toes of access holes at the bottom beam flanges for the Kobe earthquake, while brittle fracture mainly occurred at the weld root of bottom beam flanges for the Northridge earthquake due to a number of potential factors such as poor welding material, welding workmanship, connection details, and inspection quality, etc.

After the two strong earthquakes, extensive research projects were conducted in order to clarify the failure mechanisms of the brittle fracture of the welded connection and develop effective and economical design procedures to achieve more ductile performance of the connection and the structural system. It was found that the brittle fracture can be divided into three critical steps based on test results of a welded joint between a 36-mm thick cold-formed square hollow section column and a diaphragm plate with a full penetration weld under monotonic bending at room temperature (Kuwamura 1997, Kuwamura and Yamamoto 1997): (a) ductile crack initiation at a hot-spot; (b) stable ductile crack propagation; (c) explosive propagation of the cracks due to brittle fracture. Similar fracture mechanism was also verified in some SMRF bridge piers failed in the Kobe earthquake (Miki and Sasaki 2005, Usami and Ge 2009).

Recommended seismic design criteria for welded SMRF building structures were published by the Federal Emergency Management Agency (FEMA) after the Northridge earthquake based on extensive experimental and analytical results (Hamburger *et al*. 2000). The corresponding research work was mainly included in a special issue of Journal of Structural Engineering edited by Kunnath and Malley (2002). Likely, an interim guideline to prevent brittle fracture at the beam-to-column connections in welded SMRF buildings was also published by the Building Center of Japan (2003). Though extensive research efforts were devoted to brittle fracture of welded SMRF structures, there is still no effective method to predict seismic performance of welded steel structures except for experimental study, which is not only expensive but also time-consuming. For example, the fully-restrained beam-to-column connections are required to have a rotational capacity exceeding 4% radian without losing more than 20% of their maximum resistance in the FEMA design recommendations and AISC documents, and new types of connections have to pass a series of pre-qualification tests carried out using a prescribed procedure due to the fact that there is still no reliable analytical methods to accurately evaluate the ductile fracture and the followed brittle fracture of welded connections. To date, a number of studies on ductile fracture of structural steel have been carried out, e.g., (Rousselier 1987, Panontin and Sheppard 1995, Kanvinde and Deierlein 2006, Myers *et al*. 2010, Liao *et al*. 2012, Kiran and Khandelwal 2013, Jia *et al*. 2016a, Jia *et al*. 2016b) using ductile fracture models based on the concept of void growth. A number of studies on high-cycle fatigue of welded joints have also been conducted, e.g., Liu *et al*. (2014). However, limited studies on ductile fracture simulation of welds and welded connections, e.g. (Azuma *et al*. 2000, Iwashita *et al*. 2003, Myers *et al*. 2009, Qian *et al*. 2005, Qian *et al*. 2013, Qian *et al*. 2013, Wang *et al*. 2011), have been carried out due to the complexity of the problem and limitations of computational capacities when the ductile models are employed. There are several difficulties in ductile fracture simulation of welded structures in structural engineering including: (a) continuous change of material properties at the heat affected zone (HAZ) as illustrated in Fig. 1 (Mayr 2007), and lack of effective methods to calibrate the true stress-true strain data and fracture parameters up to fracture of the respective subzones; (b) too many affecting factors such as properties of base metal, welding material, heat input, etc.; (c) complicated geometrical profiles of the welds; (d) large varieties of the materials and geometrical

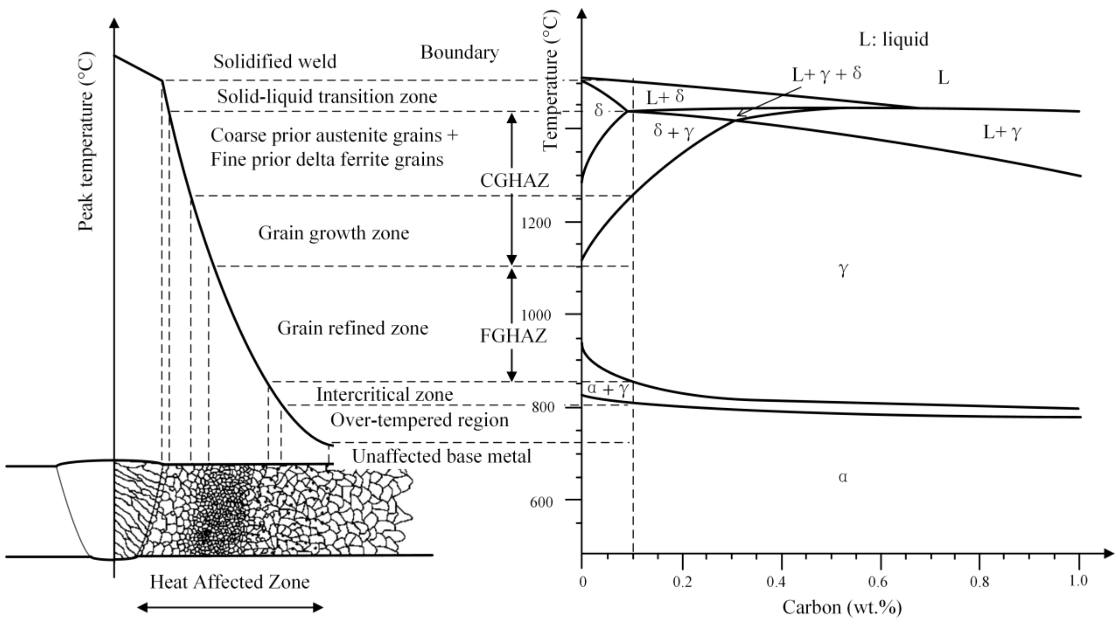

Fig. 1 Schematic illustration of various subzones of the HAZ and its correlation with the Fe-C phase diagram (adapted from Mayr 2007)

profiles depending on qualities of welding workmanship; (e) Limited available test results since engineers commonly can only obtain tensile coupon test results. The employed methods in previous studies are either difficult to apply to structural engineering due to the requirement of a number of complicated experimental tests using coupons with special configurations, or there is no standard procedure to determine the material properties.

A research program aiming at accurately simulating the ductile cracking of welded SMRF structures using proper ductile fracture and plasticity models is being carried out in the authors' laboratory. A series of large-scale experimental studies on cracking behaviors of cantilever-type columns in welded SMRF bridge piers were carried out (Ge *et al*. 2012, Luo *et al*. 2012). Ductile fracture models based on the void growth concept were respectively proposed for monotonic and cyclic loading by one of the authors, e.g., (Jia and Kuwamura 2015, Jia and Kuwamura 2013). The fracture models have been applied successfully to simulate ductile crack initiation of several types of structural steels and post-buckling fracture of square hollow section columns under both monotonic loading and cyclic large strain loading, where a two-surface plasticity model with a memory surface (Jia and Kuwamura 2013) was proposed to accurately simulate the cyclic plasticity of structural steel at extremely large plastic strain ranges. Though a lot of efforts are contributed, most former studies are focused on either the base metal of structural steel, or seismic performance of the experimentally tested connections. To date, there is no standard procedure to accurately simulate ductile cracking of welded joints.

As the first step to this complicated issue, this paper aims to present a simple and effective procedure to obtain ductile fracture parameters and true stress-true strain data of different subzones in welded joints, i.e. base metal, weld deposit, boundary, coarse-grained HAZ (CGHAZ), and fine-grained HAZ (FGHAZ). For simplicity, butt joints with single bevel groove welds are

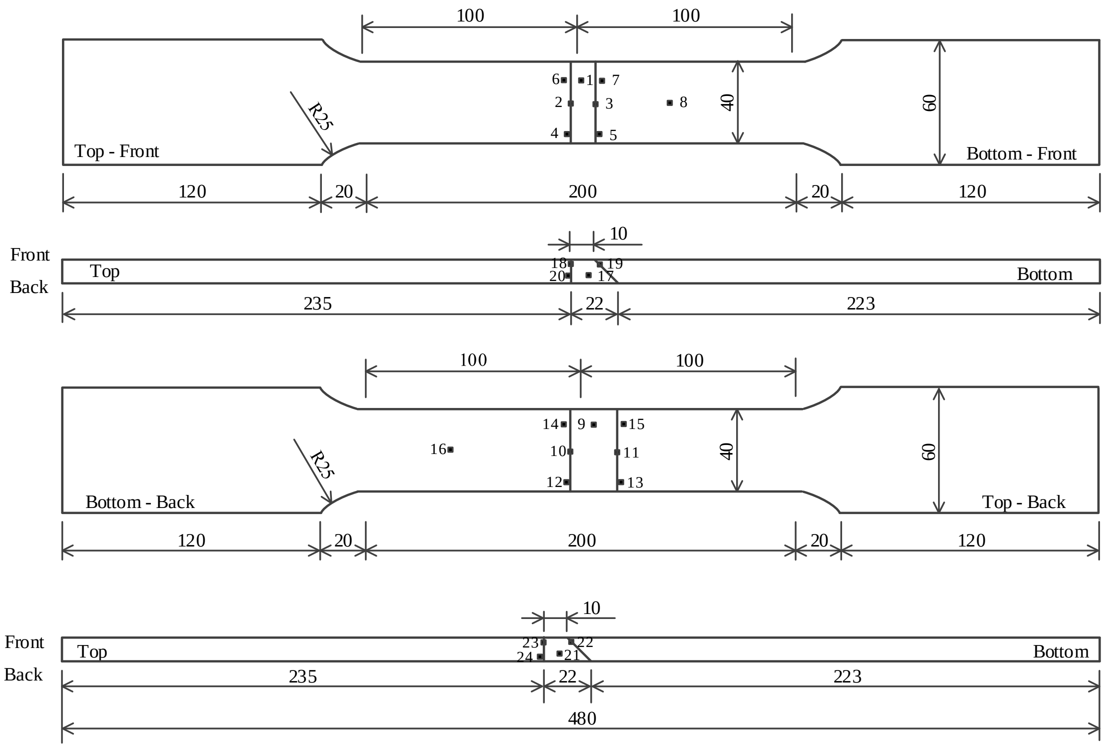

Fig. 2 Configuration of butt-welded joints without weld bead and arrangement of strain gauges

experimentally tested under monotonic tension, and the approach to obtain the fracture parameters and true stress-true strain data up to fracture is validated through comparison between experimental and numerical results. Some interesting findings are also obtained from fractographic observations using a scanning electron microscope (SEM).

2. Pull-out tests of butt joints

2.1 Configurations of butt joints

Pull-out tests on two types of butt joints with single bevel groove welds, i.e., butt joint without weld bead and U-notched joints, with the configuration as shown in Figs. 2 and 3, were conducted. The central parts of the manufactured joints are shown in Fig. 4. All the joints were manufactured from a butt-welded plate as illustrated in Fig. 5, and the surfaces of the joints near the welds were first ground and polished to smooth enough, and washed using 4% nitric acid by volume to visualize the different subzones of the welds, such as weld deposit, HAZ, base metal and their boundaries. This treatment will facilitate the observation and measurement of the accurate locations of each subzone. For the U-notched joints illustrated in Fig. 3, the notch centers were designed at the weld deposit and only 5 mm away from the left boundary, which makes it possible for the joints to crack initiate from the boundary between the weld deposit and the HAZ. The radius of the notch root is 2 mm, which is small enough to ensure cracks initiate at a location close

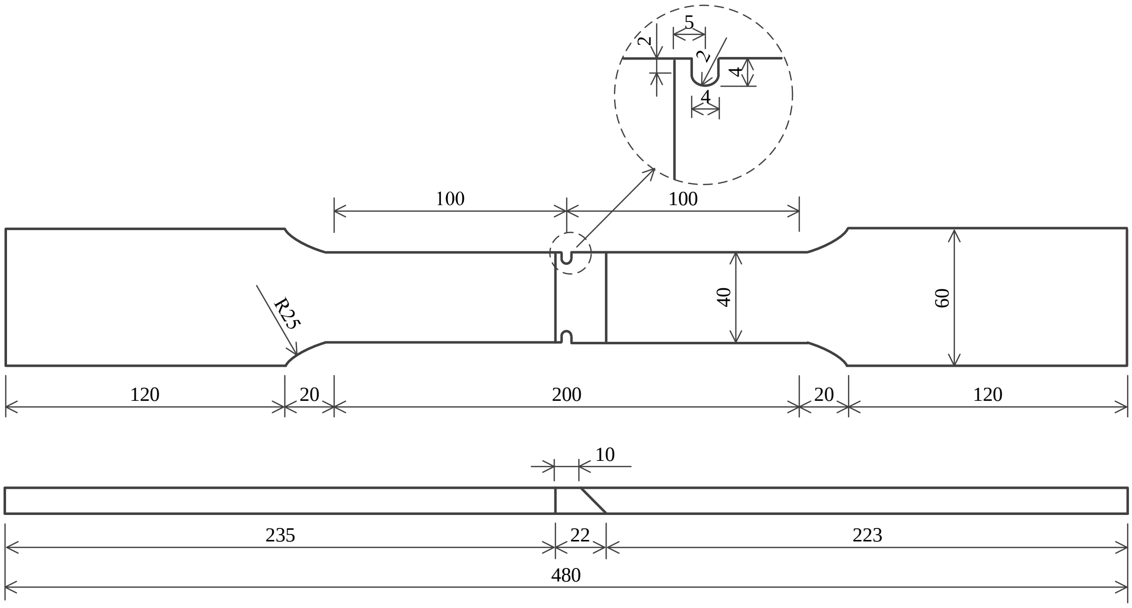

Fig. 3 Configuration of U-notched butt joints

(a) Butt joint without weld bead

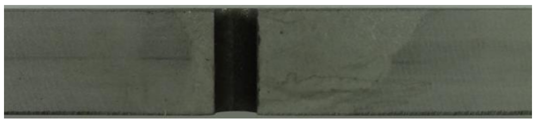

(b) U-notched butt joint

Fig. 4 Two types of butt joints

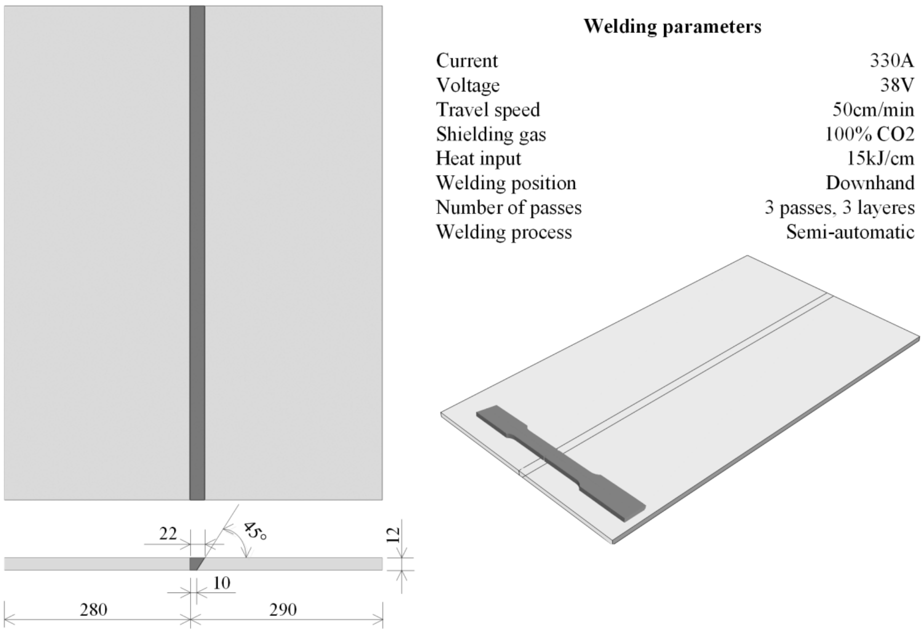

Fig. 5 Schematic illustration of welding details for the butt-welded joints

Table 1 Nominal mechanical properties and chemical compositions of base metal

Mechanical properties			Chemical compositions (% by weight)								
Yield stress (N/mm^2)	Tensile strength (N/mm^2)	Elongation (%)	C	Si	Mn	P	S	Cu	Ni	Cr	Nb
443	547	21	0.15	0.21	1.14	0.019	0.006	0.01	0.02	0.02	0.02

Table 2 Nominal mechanical properties and chemical compositions of welding electrodes

Mechanical properties				Chemical compositions (% by weight)						
Yield stress (N/mm^2)	Tensile strength (N/mm^2)	Elongation (%)	Charpy impact energy (J)	C	Si	Mn	P	S	Cu	Ti+Zr
604	659	25	132 (0℃)	0.04	0.80	1.62	0.006	0.011	0.19	0.21

Table 3 Pull-out test results of butt joints and coupons for base metal

Specimens	Displacement at crack initiation (mm)	Displacement at rupture (mm)	Load at crack initiation (kN)	Load at rupture (kN)	Maximum load (kN)	Minimum sectional area (mm^2)
J-NWB-1	31.1	31.1	205.5	205.5	248.8	457.5
J-NWB-2	32.5	32.5	199.4	199.4	243.0	462.6
J-NWB-3	27.6	27.6	203.0	203.0	240.2	440.0
J-UN-1	12.5	13.5	195.6	125.7	209.8	350.7
J-UN-2	12.5	13.0	206.4	179.8	214.8	365.1
J-UN-3	13.0	14.2	203.8	104.1	201.0	372.6
J-UN-4	12.3	13.1	190.6	90.1	201.0	333.8
CB-1	46.6	46.6	228.6	228.6	269.4	490.7
CB-2	47.0	47.0	226.8	226.8	267.8	474.8

Note: J-NWB=joints without weld bead, CB=coupons for the base metal.

to the notch surfaces but not the mid-width. A run-on and a run-off tab were employed during the welding process to avoid forming a crater on the work piece. The welding parameters are also given in the figure, where a semi-automatic welding process was employed, and the heat input is 15 kJ/cm, which is a common condition for welding in practice. Two 12-mm thick steel plates were welded along the direction perpendicular to the rolling direction using a single bevel groove weld with the bevel angle of 45 degree. The material of the plates is SM490YA, which is commonly employed in practical constructions of steel bridge structures in Japan. The material of the welding electrodes is YM-55C, and the wire diameter is 1.2 mm. The mechanical properties and chemical compositions of the base metal and the welding electrodes are respectively listed in Tables 1 and 2.

All the joints listed in Table 3 were cut along the direction as shown in Fig. 5. Totally 7 joints were manufactured, including 3 joints without weld bead (J-NWB series), and 4 U-notched joints (J-UN series). Meanwhile, two coupons (CB series) with the same configuration to that of J-NWB series were also manufactured, which were cut from the base metal before welding. The steel plates deformed due to the welding residual stress, and a straightening treatment was applied to the welded plates before cutting of the joints. This cold-forming process will increase the yield stress of the base metal, which will be discussed in the following section of coupon test results.

This study aims to outline a convenient method to characterize both the true stress-true strain data up to fracture, and the fracture parameters at different subzones in the butt joints. The coupon test results were employed to obtain the true stress-true strain data and the fracture parameter of the base metal, and the experimental and numerical results of the joints without weld bead were used to determine the true stress-true strain data at the weld deposit, boundary, CGHAZ, FGHAZ, and the corresponding fracture parameter of the region where crack initiated. Meanwhile, numerical simulation using the ductile fracture model was carried out to validate the applicability of the model to welds. The experimental and numerical tests of the U-notched joints were employed to verify the obtained true stress-true strain data, and also to calibrate the fracture parameter at the weld deposit, i.e. to validate the whole procedure.

2.2 Test setup and arrangement of strain gauges

The pull-out test setup for all the joints is the same as illustrated in Fig. 6 by a U-notched joint, where a universal tensile testing machine with the maximum load capacity of 2000 kN was employed. Elongations of the joints were measured using a specially designed extensometer, PI-60S-200, with a large displacement capacity of 60 mm provided by Tokyo Measuring Instruments Laboratory. The extensometer can measure the extension up to rupture for all the joints, which is of great importance in this study. The gage length for all the joints and coupons is 200 mm as shown in the figure. Three video cameras were respectively focused at the two side surfaces, and front surface to monitor necking, crack initiation and propagation.

Twenty-four strain gauges with the arrangement as illustrated in Fig. 2 were employed to measure the strain up to necking of the joint without weld bead. The type of the strain gauges is YFLA-2, which is commonly used for large plastic straining, and the strain capacity is around 20%. The strain gauges can well capture the strain data up to necking initiation of the joints and coupons, since necking commonly initiates at around 20% for virgin structural steel. The arrangement of the strain gauges is as follows, (a) weld deposit: Gauges 1, 9, 17 and 21; (b) boundary: Gauges 2, 3, 10, 11, 18, 19, 22 and 23; (c) CGHAZ: Gauges 4, 5, 12, 13, 20 and 24; (d) FGHAZ: Gauges 6, 7, 14 and 15; (e) base metal: Gauges 8 and 16. Besides, all the tests were carried out in room temperature at a quasi-static speed, where each test averagely takes 1 to 2 hours to monitor the crack initiation and propagation.

2.3 Test results

The test results of all the joints and the coupons at the base metal are listed in Table 3. The failure modes of the joints without weld bead can be found in Fig. 7, where necking first started at the weld deposit and induced strain concentration, and finally rupture occurred abruptly at the necked region close to the weld deposit and the boundary part. The detailed crack initiation location cannot be verified by human eyes or digital cameras due to the irregular fracture surface and profile of the weld, so fractographic study using a scanning electron microscope (SEM) was conducted to analyze the detailed crack initiation location of the joints without weld bead in a following section.

The load-displacement curves of the three joints without weld bead are plotted in Fig. 8, where the displacements at rupture are respective 31.1, 32.5 and 27.6 mm. Surface grinding was applied

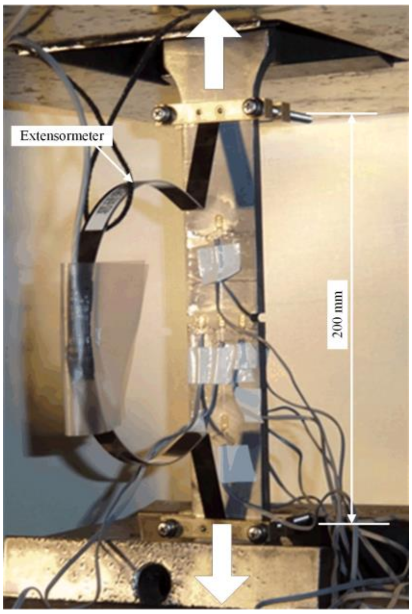

Fig. 6 Setup of U-notched joint

Fig. 7 Necking and final cracking at the weld deposit of the butt joint without weld bead

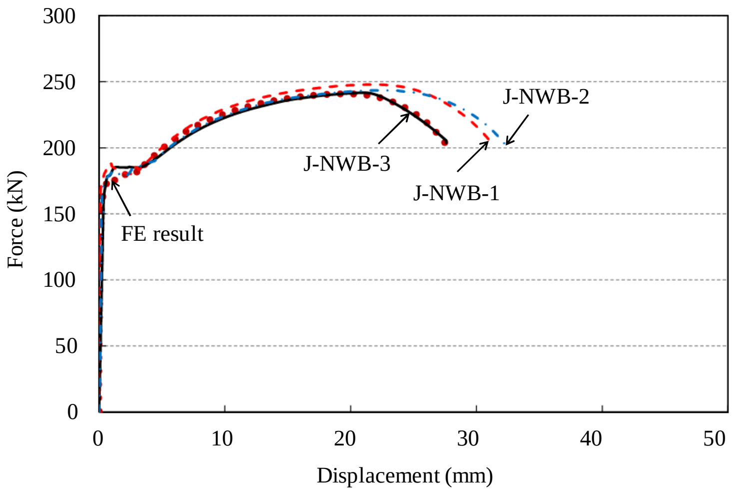

Fig. 8 Comparison of load-displacement curves for the butt joint without weld bead

to the whole length of Joint J-NWB-3 to facilitate the measurement and monitoring. The maximum load is therefore lower than those of the other two joints without surface treatment. The data of the strain gauges at the weld deposit, boundary, CGHAZ and FGHAZ are respectively given in Figs. 9 (a) to (d). Due to the complex profile of the welds, there are some deviations for different strain gauges. It was found that the strain data at the side surfaces are more accurate than those at the front and back surfaces, which can be found in Figs. 9(a) to (c).

Crack first initiated at the mid-thickness of the notch root surface for the U-notched joints as

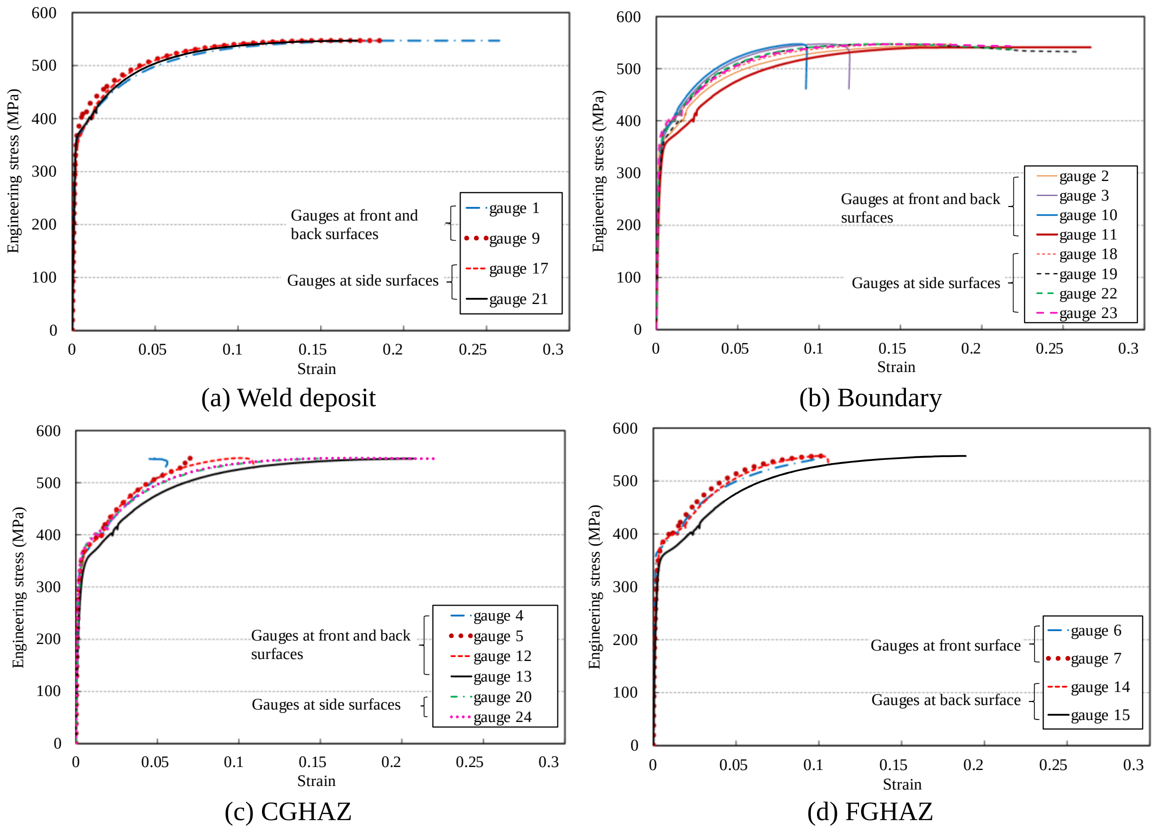

(a) Weld deposit (b) Boundary

(c) CGHAZ (d) FGHAZ

Fig. 9 Stress-strain data of each subzone obtained from strain gauges

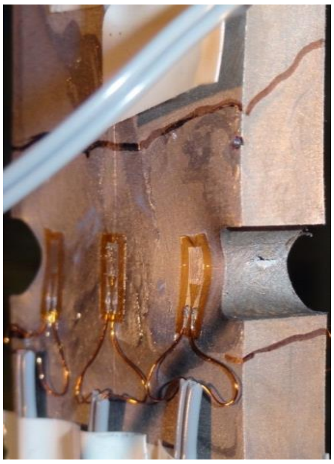

Fig. 10 Crack initiation at notch root surface of U-notched joint

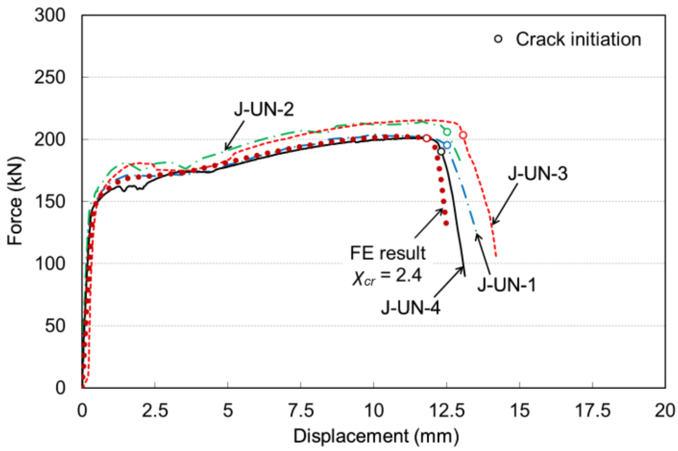

Fig. 11 Comparison of load-displacement curves for U-notched butt joints

illustrated in Fig. 10, and propagated approximately horizontally along the width direction quickly after the crack initiation. The load-displacement curves of the four U-notched joints are shown in

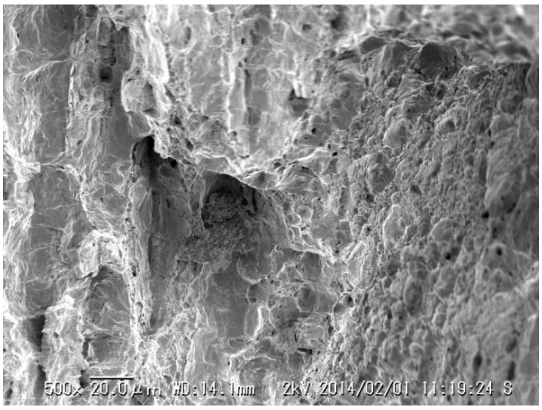

Fig. 12 Fracture surfaces of base metal using an SEM

Fig. 11, where the curves are close to each other. The instants at crack initiation and rupture are also close to each other. Compared with the joints of J-NWB series, the U-notched joints have relative small rupture displacements, which are approximately half of those of the notchless joints. The test results also indicate that crack initiation and propagation of the U-notched joints with proper radius at the notch root are not sensitive to manufacturing deviations, which is more reliable to be employed to calibrate the model parameters of ductile fracture models compared with sharply-notched ones.

2.4 Fractographic study

Fractographic observation was carried out to investigate microstructures of different regions in the welded joints, and to verify the accurate locations of crack initiation for the joints without weld bead. A typical ductile fracture surface with a dimple pattern at the base metal is shown in Fig. 12, where the size of a large dimple at the center of the figure is approximate 0.05 mm, and the surrounding dimples are relative small. Fracture surfaces at Points "A" and "B" as shown in Fig. 13(a) observed using an SEM for the joints without weld bead are shown respectively in Figs. 14(a) and (b). The fracture surface at Point "A" is a typical dimple pattern, with the dimple size of around 0.01 mm, which is relative small compared with the base metal. Based on the comparison of different locations at the weld deposit, the material at Point "A" was verified as the weld deposit. However, a different microstructure was found at Point "B" as shown in Fig. 14(b), where a layer of second phase particles were observed. It can be inferred that Point "B" is within the boundary part between the weld deposit and the HAZ. Therefore, crack initiated at the boundary part for the joints without weld bead, and the different microstructures at the boundary result in a poor ductility of the joints. As shown in Fig. 1, the boundary part is subjected to peak temperature during a welding process, which will greatly deteriorates the fracture toughness of the material. Three points, "C", "D" and "E" of the U-notched joints as shown in Fig. 13(b) were observed using an SEM, where the appearance at the center of the surface is different from the other parts. The SEM observation results for Points "C", "D" and "E" are respectively shown in Figs. 15(a) to (c). All the three points are located within the weld deposit, and a typical dimple pattern similar to Fig. 14(a) was found at Point "C" near the notch, indicating a ductile fracture mechanism. A quasi-cleavage fracture surface was verified at Point "E", where a mixture of cleavage fracture and void

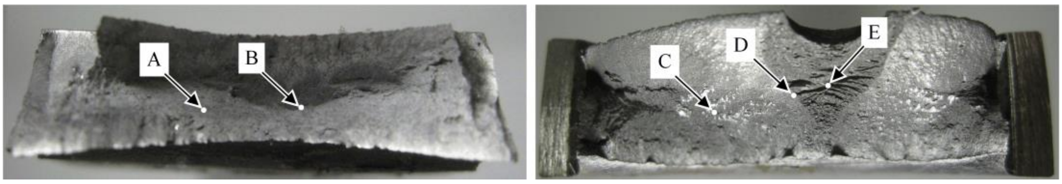

(a) Joint without weld bead (b) U-notched joint

Fig. 13 Typical fracture surfaces of joints without weld bead and U-notched joints taken by a digital camera

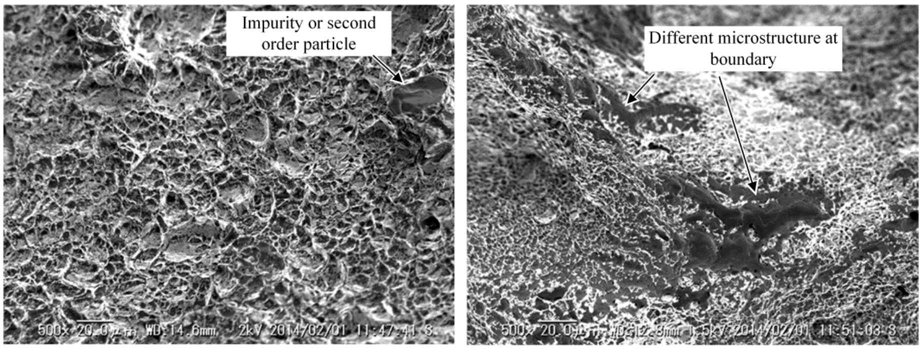

(a) Dimple pattern at Point A (b) Fracture surface at Point B

Fig. 14 Fracture surfaces of joints without weld bead using an SEM

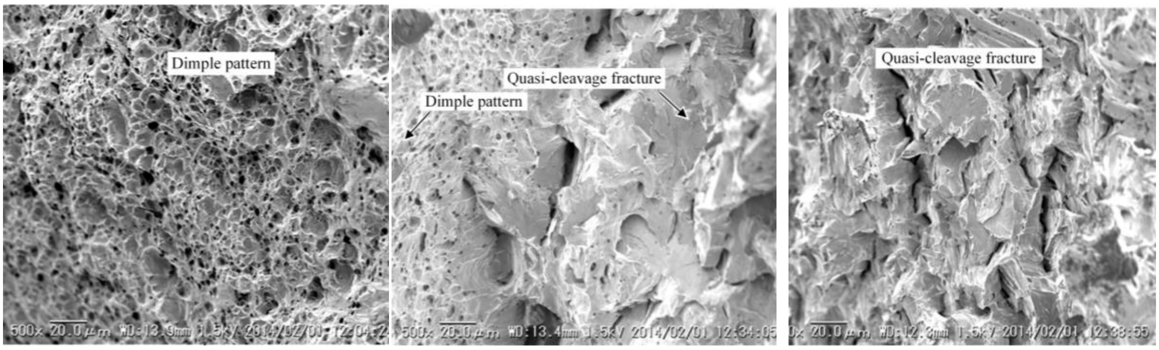

(a) Dimple pattern at Point C (b) Transition of fracture modes at Point C (c) Quasi-cleavage fracture at Point E

Fig. 15 Fracture surfaces of U-notched joints using an SEM

coalescence fracture can be found. Unlike a typical river pattern observed in a cleavage fracture surface (brittle fracture), the directions of the quasi-cleavage fracture are disturbed by dimples as shown in Fig. 15(c). Transition from a dimple pattern to quasi-cleavage fracture was observed at Point "D". The main difference of the three points is the distance from the crack initiation point (the right notch root at Fig. 13(b)). Therefore, the main factor to induce the transition of the fracture mechanisms is the crack length, where a larger crack length induces more severe stress concentration at the crack tips during the crack propagation, and a severe stress concentration makes the material more susceptible to quasi-cleavage and cleavage fracture.

3. Numerical simulation

3.1 Ductile fracture model under monotonic tension

A ductile fracture model based on the void growth model proposed by Rice and Tracey (1969) and the critical void growth index (McClintock 1968) was employed by one of the authors (Jia and Kuwamura 2013). The relationship between the radius of a void and stress triaxiality based on a simplified model of a spherical void in a remote simple tension strain rate field. The void growth rate for Mises materials can be given as

$$\frac{\mathrm{d}R}{R} = 0.283 \cdot e^{\frac{3}{2}\frac{\sigma_h}{\sigma_{eq}}} \mathrm{d}\varepsilon_{eq} = 0.283 \cdot e^{\frac{3}{2}T} \mathrm{d}\varepsilon_{eq} \tag{1}$$

where R is the average radius of the void, and σ_h and σ_{eq} are hydrostatic stress and equivalent stress respectively; T is stress triaxiality and $\mathrm{d}\varepsilon_{eq}$ is incremental equivalent strain. However, the Rice-Tracey model has no criterion for void coalescence. Integrating Eq. (1), one can obtain

$$\ln \frac{R}{R_0} = 0.283 \int_0^{\varepsilon_{eq}} e^{\frac{3}{2}T} \mathrm{d}\varepsilon_{eq} \tag{2}$$

where R_0 is the initial radius of the void. Based on a term of critical void growth index (Kanvinde and Deierlein 2006, Panontin and Sheppard 1995, Rousselier 1987), χ_{cr}, void coalescence is postulated to occur when R/R_0 reaches a critical value. For the case when the stress triaxiality is constant, the relationship between fracture strain (equivalent strain) and stress triaxiality can be given.

$$\varepsilon_f = \ln \frac{R_f}{R_0} / (0.283 e^{\frac{3}{2}T}) = \chi_{cr} \cdot e^{-\frac{3}{2}T} \tag{3}$$

where ε_f and R_f are fracture strain and the corresponding radius, and χ_{cr} is a model parameter defining the threshold value for void growth.

In order to extend the above equation to the case of general loading associates with non-constant stress triaxialities, the Miner's rule (Miner 1945) is employed to apply the model to various loading histories. If T is assumed to be constant during a single incremental step, the incremental damage due to incremental strain $d\varepsilon_{eq}$ can be defined according to the Miner's rule as

$$\mathrm{d}D = \frac{\mathrm{d}\varepsilon_{eq}}{\varepsilon_f(T)} = \frac{\mathrm{d}\varepsilon_{eq}}{\chi_{cr} \cdot e^{-\frac{3}{2}T}} \tag{4}$$

where D is a damage index and a material is postulated to fracture when D reaches unit. Assuming that damage is only resulted by plastic deformation, Eq. (4) can be written as

$$\mathrm{d}D \approx \frac{\mathrm{d}\varepsilon_{eq}^{p}}{\chi_{cr} \cdot e^{-\frac{3}{2}T}} \tag{5}$$

This ductile fracture model has been validated by experimental results of several types of structural virgin steels, and this paper aims to study the applicability of the model to pull-out tests

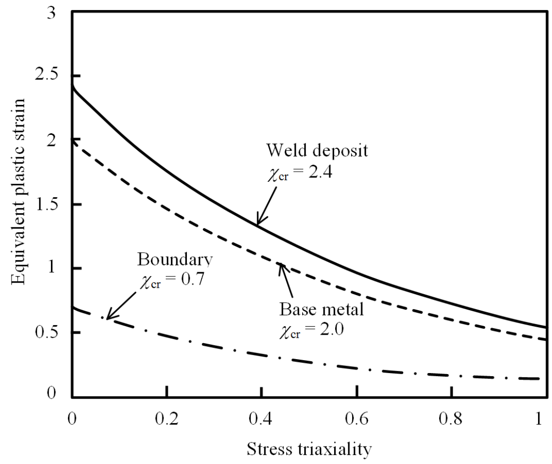

Fig. 16 Fracture strain versus stress triaxiality curves for different locations

of welds. The model parameter, χ_{cr}, can be calibrated using only monotonic tensile coupon test or smoothly-notched coupon test results through several iterations of numerical simulations with the implemented fracture model. Before the calibration of the fracture parameter, one has to first obtain the true stress-true strain data up to fracture of the material, which will be inputted during the numerical calibration of the fracture parameter, since the fracture model is based on the local stress parameter, T, and strain parameter, ε_{eq}. A validated method to obtain the true stress-true strain data up to fracture will be employed in the following section, and the obtained data were employed in the calibrations of the fracture parameters for materials at different regions. The calibrated value for χ_{cr} is 2.0 for the base metal, and those of the boundary and weld deposit were respectively obtained using the test results of the joint without weld bead and U-notched joints. The fracture strain versus the stress triaxiality curves for the materials were presented in Fig. 16. The fracture parameters of the other regions cannot be obtained in this study since no fracture occurred in the corresponding parts. Specially designed smoothly-notched coupons are required to obtain the corresponding fracture parameters. However, it will not affect generality of the proposed model and corresponding calibration method. Ductile fracture simulation can be carried out without difficulty once the true stress-true strain data of the materials at all the regions are obtained, and the fracture parameters at the regions of crack initiation in the tests are also known.

3.2 True stress-true strain data up to fracture at different regions

There are some difficulties in obtaining the true stress-true strain data up to fracture, since necking will occur at a smooth tensile coupon, and the stress state will become triaxial after necking initiation but not uniaxial. There is no accurate theoretical method to obtain the true stress and true strain data after necking initiation for hardening materials such as mild steels. A simple modified weighted average method was proposed by one of the authors (Jia and Kuwamura 2013), which postulates that the true stress-true strain curve after necking initiation is approximately linear. The method was successfully applied to several structural steels. A power law tangent method was also proposed to estimate the post-necking true stress-true strain relationship of different structural steels, especially for high strength steel. It has been found that there is minor

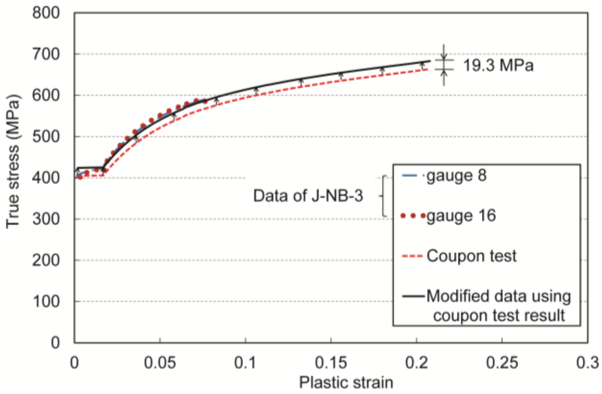

Fig. 17 Modified true stress-true strain data for the base metal after straightening

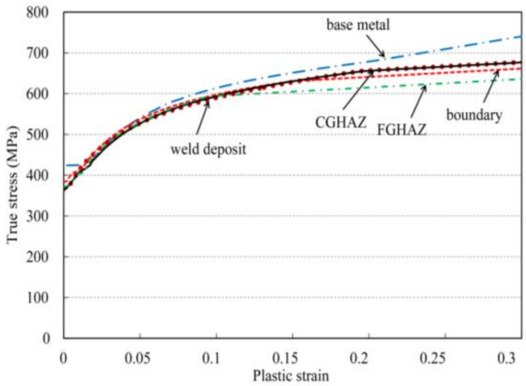

Fig. 18 Input true stress-true strain data at different locations

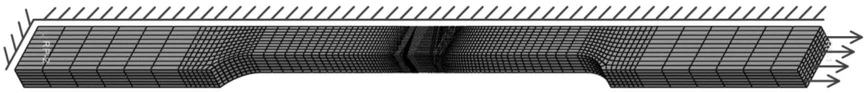

(a) Half model

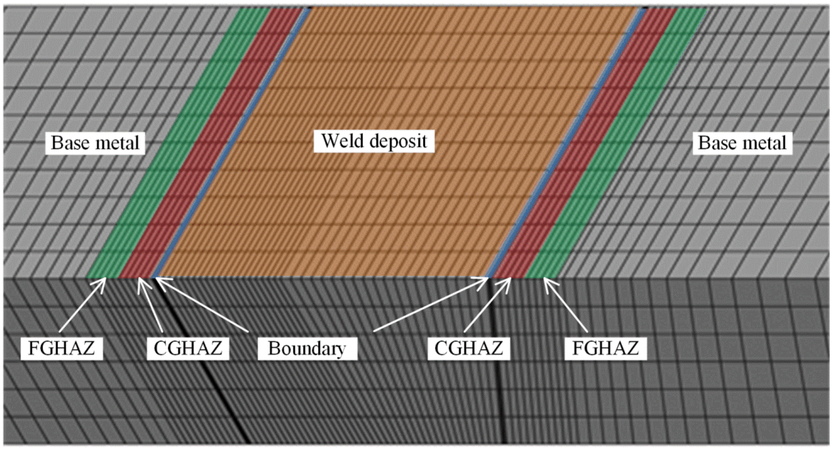

(b) Simulation of weld

Fig. 19 FE modeling of the butt joint without weld bead

deviation for the calibrated fracture parameter when the two methods are employed. For simplicity, the modified weighted average method was also employed in this study for the materials at different regions.

It was found that the stress data from the base metal of the joints were higher than those obtained from the coupon test results, which is mainly due to the straightening process after the welding. Therefore, the true stress-true strain data obtained from the strain gauges at the base metal of the joints are more accurate, while the corresponding data up to necking are not available due to premature necking at the weld deposit. Therefore, the true stress-true strain data obtained from the coupon tests were modified to fit the true stress-true strain data of the base metal after straightening as shown in Fig. 17. The true stress-true strain data up to fracture at different regions are compared in Fig. 18, which are adopted as the input data for the fracture simulations.

3.3 FE modeling

Ductile fracture of all the joints and the coupons was simulated by element deletion method in ABAQUS/ Explicit (2011) (ABAQUS 2011), and three dimensional solid elements *C3D8R* were employed to carry out the quasi-static simulations. Half models were used to improve the computational efficiency, and the mesh of the joint without weld bead is illustrated in Fig. 19. The joint was divided into several regions, i.e., weld deposit, boundary, CGHAZ, FGHAZ and base metal. The sizes of the weld and HAZ were measured from the actual joints, and the size of the boundary was set as 0.25 mm according to the hardness test results in the literature (Zhou 2009). Convergence studies were also carried out for each simulation to determine proper sizes for the FE model. For the U-notched specimens, the typical mesh size at the notch root is about 2 mm, which is fine enough to ensure the convergence of the analysis. The analysis time for each model was set long enough to ensure the analysis be quasi-static. Since the tests are all under monotonic loading, an isotropic hardening plasticity model is employed for the current simulations. Cracking of the specimens was simulated using the element deletion method according to Eq. (5), and an element is removed when the damage index reaches one.

3.4 Comparison between experimental and numerical results

The numerical simulation results for the joint without weld bead are shown in Fig. 20. The failure process of the joint without weld bead was well simulated, where necking first occurred at the weld deposit, and ductile crack initiated at the necked region. The stress triaxiality and equivalent plastic strain contour plots are shown in Fig. 20, where crack initiates at the boundary part in the simulation. Fig. 20(a) also implies that stress triaxiality can concentrate at the boundary

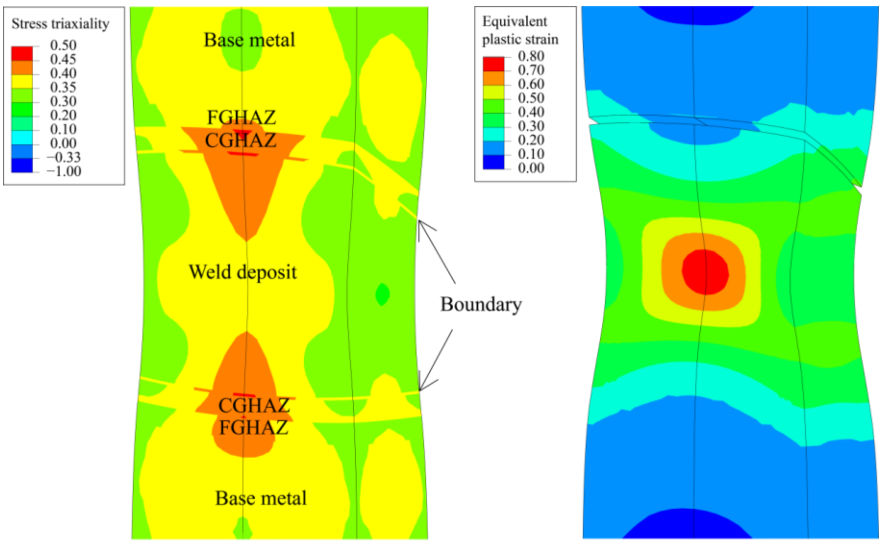

(a) Stress triaxiality (b) Equivalent plastic strain

Fig. 20 Contour plots for the joint without weld bead

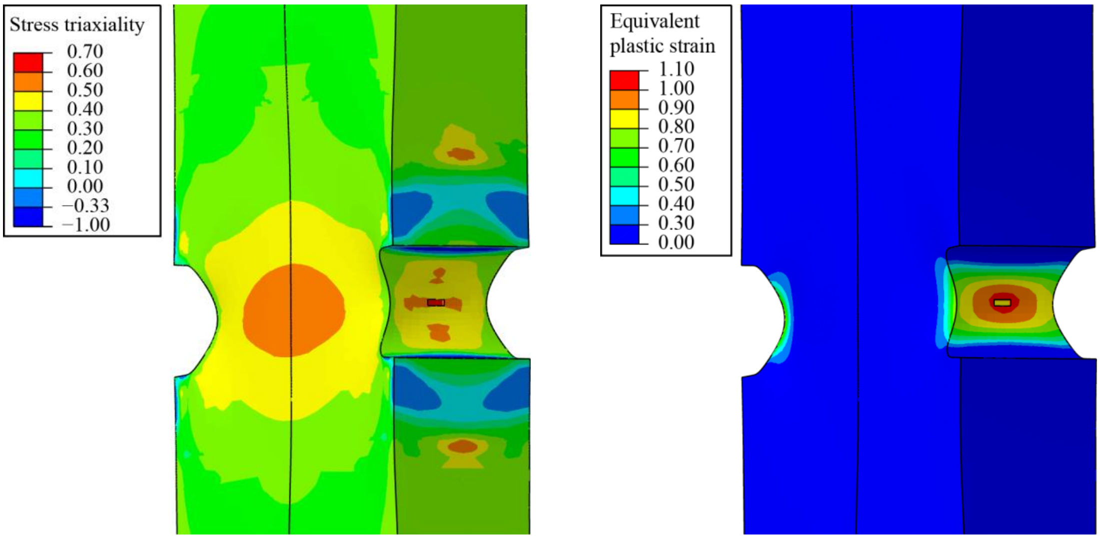

(a) Stress triaxiality (b) Equivalent plastic strain

Fig. 21 Crack initiation simulation result for U-notched butt joint

between two materials nearby the weld, which was termed material notch in the literature (Zhou 2009). The material notch effect can induce premature fracture at the corresponding boundaries between two materials, since a larger positive stress triaxiality is associated with smaller fracture strain according to Eq. (5). The load-displacement curves of the experiments are evaluated with good accuracy by the numerical simulation as shown in Fig. 8, indicating that the material characterization procedure and the ductile fracture model are successfully applied to the welded joints.

The comparison results of the load-displacement curves and ductile crack initiation for U-notched joints are respectively shown in Fig. 11, Fig. 10 and Fig. 21, where the analysis result compares well with the test results. The crack initiation at the mid-thickness of the notch root surface is well predicted by the numerical results as illustrated in Fig. 10 and Fig. 21. The contour plots also indicate that the stress triaxiality concentrates at both the center and notch root of the joint, and strain only concentrates at the notch root surface. The crack thus first initiated at the notch root surface but not the center according to Eq. (5). This implies that the commonly employed damage evaluation method using either equivalent plastic strain or stress triaxiality as an index sometimes may give an inaccurate predicted location of crack initiation.

4. Discussion

This paper investigates a procedure to conduct ductile cracking simulation of welded joints, where simple butt joints under monotonic tension were employed to illustrate the whole validation procedure. The subzones, i.e., base metal, weld deposit, boundary, CGHAZ and FGHAZ, at the welds are commonly too narrow to measure the true stress-true strain data, especially for the boundary and HAZ parts. Fortunately, it is indicated by the stress-strain data shown in Fig. 18 that the differences among the different subzones are minor, and one may utilize the stress-strain data of the base metal to describe the ones of the boundary, CGHAZ and FGHAZ if there is no accurate experimental data of the three narrow subzones provided.

The stress states are tension dominant, and a VGM is thus applicable to the test results. For the other stress states where shear loading is dominant, the VGM may not perform well, and more experimental and theoretical studies are required. In addition, the joints investigated in this study all cracked quickly, which is similar to that of a smooth coupon under monotonic tension. Under this condition, the element deletion method assuming that an element is removed when the damage index, D, reaches unit, works well for the cracking simulation, and the elements at the minimum sections reaches the damage limit state at almost the same time. However, for other cases such as deeply-notched specimens where crack propagation takes a large portion of the elongation, the element deletion method may greatly underestimate the deformation capacity of the specimens, and further study is required. Since the main focus of this study is on crack initiation, this issue is not the concern of this paper.

5. Conclusions

A material characterization procedure to obtain the true stress-true strain data up to fracture was presented to obtain the material properties of different regions in welded structural steel joints in this paper. Experiments on butt joints with and without weld bead, and U-notched joints were conducted. Numerical simulations using the obtained true stress-true strain data and a micro-mechanical ductile fracture model were carried out. The main conclusions are given as follows.

- The material characterization method using strain gauges with large strain capacities and a previously proposed modified weighted average method can be well applied to weld deposit and the subzones within heat affected zone (HAZ) in order to obtain their true stress-true strain data up to fracture.
- Joints without weld bead are susceptible to ductile failure initiating at the boundary between the base metal and HAZ.
- Transition from dimple pattern to quasi-cleavage fracture was verified from the fractographic study of the U-notched joints, which is mainly induced by severe stress concentration at crack tips when a ductile crack length grows to a threshold value.
- The ductile fracture model can be employed to predict the crack initiation of butt joints with good accuracy if proper material characterization methods are employed.
- Material inhomogeneity can result in stress triaxiality concentration at a boundary of two different materials, which may induce premature failure of welded structures.

The ductile failure problem of welded structures is very complicated, which can be affected by a number of factors. Unified stress-strain relationships for the materials at different regions of welds are required to establish a more convenient evaluation method. Meanwhile, the applicability of the current method and fracture model to failure analysis of more complicated welded steel connections has to be further validated in future.

Acknowledgments

The study is supported in part by grants from the Advanced Research Center for Natural Disaster Risk Reduction, Meijo University, which supported by Ministry of Education, Culture, Sports, Science and Technology (MEXT), Japan. The first author is thankful for financial support by the National Natural Science Foundation of China (Grant No. 51508401). The third author is thankful for financial support from the JSPS postdoctoral fellowship program for foreign researchers (Grant No. 12067). The experimental support for the fractographic study from Dr. Araki, Dr. Koyama and Prof. Kuwamura are greatly appreciated.

References

ABAQUS (2011), ABAQUS/Analysis User's Manual-version 6.9, ABAQUS, Inc., Pawtucket, Rhode Island.

AIJ (1995), *Fracture in steel structures during a severe earthquake*, Tokyo, Japan.

Azuma, K., Kurobane, Y. and Makino, Y. (2000), "Cyclic testing of beam-to-column connections with weld defects and assessment of safety of numerically modeled connections from brittle fracture", *Eng. Struct.*, **22**(12), 1596-1608.

Bruneau, M., Wilson, J.C. and Tremblay, R. (1996), "Performance of steel bridges during the 1995 Hyogo-ken Nanbu (Kobe, Japan) earthquake", *Can. J. Civ. Eng.*, **23**(3), 678-713.

Building Center of Japan (2003), *Guidelines for prevention of brittle fracture at the beam ends of welded beam-to-column connections in steel frames*, Tokyo, Japan.

Ge, H., Kang, L. and Tsumura, Y. (2012), "Extremely low-cycle fatigue tests of thick-walled steel bridge piers", *J. Bridge Eng.*, ASCE, **18**(9), 858-870.

Hajjar, J.F., Gourley, B.C., O'Sullivan, D.P. and Leon, R.T. (1998), "Analysis of mid-rise steel frame damaged in Northridge earthquake", *J. Perform. Constr. Facil.*, ASCE, **12**(4), 221-231.

Hamburger, R.O., Hooper, J.D., Sabol, T., Shaw, R., Reaveley, L.D. and Tide, R.H.R. (2000), *Recommended seismic design criteria for new steel moment-frame buildings (fema-350)*, FEMA-350. SAC Joint Venture, Federal Emergency Management Agency, Washington D.C.

Iwashita, T., Kurobane, Y., Azuma, K. and Makino, Y. (2003), "Prediction of brittle fracture initiating at ends of CJP groove welded joints with defects: study into applicability of failure assessment diagram approach", *Eng. Struct.*, **25**(14), 1815-1826.

Jia, L.J. and Kuwamura, H. (2013a), "Ductile fracture simulation of structural steels under monotonic tension", *J. Struct. Eng.*, ASCE, **140**(5), 04013115.

Jia, L.J. and Kuwamura, H. (2013b), "Prediction of cyclic behaviors of mild steel at large plastic strain using coupon test results", *J. Struct. Eng.*, ASCE, **140**(2), 04013056.

Jia, L.J. and Kuwamura, H. (2015), "Ductile fracture model for structural steel under cyclic large strain loading", *J. Constr. Steel Res.*, **106**, 110-121.

Jia, L.J., Ikai, T., Ge, H.B., Shinohara, K. and Kato, H. (2016a), "Experimental and numerical study on ductile fracture of structural steels under combined shear and tension", *J. Bridge Eng.*, ASCE, **21**(5), 04016008.

Jia, L.J., Ikai, T., Shinohara, K. and Ge, H.B. (2016b), "Ductile crack initiation and propagation of structural steels under cyclic combined shear and normal stress loading", *Constr. Build. Mater.*, **112**, 69-83.

Kanvinde, A.M. and Deierlein, G.G. (2006), "Void growth model and stress modified critical strain model to predict ductile fracture in structural steels", *J. Struct. Eng.*, ASCE, **132**(12), 1907-1918.

Kiran, R. and Khandelwal, K. (2013), "Experimental studies and models for ductile fracture in ASTM A992 steels at high triaxiality", *J. Struct. Eng.*, ASCE, **140**(2), 04013044.

Kunnath, S.K. and Malley, J.O. (2002), "Advances in seismic design and evaluation of steel moment frames: recent findings from FEMA/SAC Phase II Project", *J. Struct. Eng.*, ASCE, **128**(4), 415-419.

Kuwamura, H. (1997), "Transition between fatigue and ductile fracture in steel", *J. Struct. Eng.*, ASCE, **123**(7), 864-870.

Kuwamura, H. and Yamamoto, K. (1997), "Ductile crack as trigger of brittle fracture in steel", *J. Struct. Eng.*, ASCE, **123**(6), 729-735.

Lab, K. (1998), "Field survey report on structural damage during the 1995 Hyogoken-Nanbu Earthquake", The University of Tokyo, Tokyo, Japan.
Liao, F., Wang, W. and Chen, Y. (2012), "Parameter calibrations and application of micromechanical fracture model of structural steels", *Struct. Eng. Mech.*, **42**(2), 153-174.
Liu, Y., He, C., Huang, C., Khan, M.K. and Wang, Q. (2014), "Very long life fatigue behaviors of 16Mn steel and welded joint", *Struct. Eng. Mech.*, 5**2**(5), 889-901.
Luo, X.Q., Ge, H.B. and Ohashi, M. (2012), "Experimental study on ductile crack initiation in compact section steel columns", *Steel Compos. Struct.*, **13**(4), 383-396.
Mahin, S.A. (1998), "Lessons from damage to steel buildings during the Northridge earthquake", *Eng. Struct.*, **20**(4-6), 261-270.
Mayr, P. (2007), "Evolution of microstructure and mechanical properties of the heat affected zone in B-containing 9% chromium steels", Doctoral Dissertation, Graz University of Technology, Austria.
McClintock, F.A. (1968), "A criterion for ductile fracture by the growth of holes", *J. Appl. Mech.*, **35**, 363.
Miki, C. and Sasaki, E. (2005), "Fracture in steel bridge piers due to earthquakes", *Int. J. Steel Struct.*, **5**(2), 133-140.
Miner, M.A. (1945), "Cumulative damage in fatigue", *J. Appl. Mech.*, **12**(3), A159-A164.
Myers, A.T., Kanvinde, A.M. and Deierlein, G.G. (2010), "Calibration of the SMCS criterion for ductile fracture in steels: specimen size dependence and parameter assessment", *J. Eng. Mech.*, ASCE, **136**(11), 1401-1410.
Myers, A.T., Kanvinde, A.M., Deierlein, G.G. and Fell, B.V. (2009), "Effect of weld details on the ductility of steel column baseplate connections", *J. Constr. Steel Res.*, **65**(6), 1366-1373.
Nakashima, M., Inoue, K. and Tada, M. (1998), "Classification of damage to steel buildings observed in the 1995 Hyogoken-Nanbu earthquake", *Eng. Struct.*, **20**(4), 271-281.
O'Sullivan, D.P., Hajjar, J.F. and Leon, R.T. (1998), "Repairs to mid-rise steel frame damaged in Northridge earthquake", *J. Perform. Constr. Facil.*, ASCE, **12**(4), 213-220.
Panontin, T.L. and Sheppard, S.D. (1995), "The relationship between constraint and ductile fracture initiation as defined by micromechanical analyses", *Proceedings of the Fracture mechanics: 26th Volume*, ASTM STP 1256, ASTM, West Conshohoken, ASTM, 54.
Qian, X., Choo, Y., Liew, J. and Wardenier, J. (2005), "Simulation of ductile fracture of circular hollow section joints using the Gurson model", *J. Struct. Eng.*, ASCE, **131**(5), 768-780.
Qian, X., Li, Y. and Ou, Z. (2013), "Ductile tearing assessment of high-strength steel X-joints under in-plane bending", *Eng. Fail. Anal.*, **28**, 176-191.
Qian, X., Zhang, Y. and Choo, Y.S. (2013), "A load-deformation formulation with fracture representation based on the J-R curve for tubular joints", *Eng. Fail. Anal.*, **33**, 347-366.
Rice, J. and Tracey, D.M. (1969), "On the ductile enlargement of voids in triaxial stress fields", *J. Mech. Phys. Solid.*, **17**(3), 201-217.
Rousselier, G. (1987), "Ductile fracture models and their potential in local approach of fracture", *Nucl. Eng. Des.*, **105**(1), 97-111.
Usami, T. and Ge, H.B. (2009), "A performance-based seismic design methodology for steel bridge systems", *J. Earthq. Tsunami*, **3**(3), 175-193.
Wang, H., Wang, G., Xuan, F. and Tu, S. (2011), "Numerical investigation of ductile crack growth behavior in a dissimilar metal welded joint", *Nucl. Eng. Des.*, **241**(8), 3234-3243.
Zhou, Z.G. (2009), "A study on fracture of steel beam-to-column welded connections", Doctoral Dissertation, The University of Tokyo, Tokyo, Japan.

CC